Author Manuscript

Author Manuscript

Author Manuscript

Author Manuscript

HHS Public Access

Author manuscript

Biomech Model Mechanobiol. Author manuscript; available in PMC 2016 June 01.

Published in final edited form as:

Biomech Model Mechanobiol. 2015 June ; 14(3): 589–602. doi:10.1007/s10237-014-0624-2.

Cardiomyocyte subdomain contractility arising from microenvironmental stiffness and topography

Kathleen M Broughton[1] and **Brenda Russell**[2]

[1]Department of Bioengineering, University of Illinois at Chicago, Chicago, Illinois, USA

[2]Department of Physiology and Biophysics, University of Illinois at Chicago, Chicago, Illinois 60612 USA

Abstract

Cellular structure and function are interdependent. To understand this relationship in beating heart cells, individual neonatal rat ventricular myocytes (NRVM) were analyzed one and three days after plating when cultured on different stiffness (100 kPa, 400 kPa) and surface structures (flat or 15 μm-high, 15 μm-diameter, microposts spaced 75 μm apart) manufactured from polydimethylsiloxane (PDMS). Myofibril structure seen by immunohistochemistry was organized in three dimensions when NRVMs were attached to microposts. On day three, paxillin distribution near the post serving as cellular anchorage was quantified on both soft posts (12.04% of total voxel count) and stiff posts (8.16%). Living NRVM were analyzed using line scans for sarcomeric shortening and shortening velocity, and traction force microscopy for surface stress and surface tension. One day after plating, NRVMs shortened more on soft posts (1.08 μm at 4.75 μm/s) compared to either soft flat (0.84 μm at 3.41 μm/s), stiff posts (0.66 μm at 2.88 μm/s) or stiff flat (0.48 μm at 1.44 μm/s). NRVMs have decreased shortening and shortening velocity on soft posts (1.04 μm at 3.85 μm/s) compared to soft flat (0.72 μm at 2.36 μm/s) substrates. The surface stress and surface tension, increased over time for both soft post (29.12 kN/m^2 and 30.10 μN/mm to 42.87 kN/m^2 and 51.68 μN/mm) and flat (15.36 kN/m^2 and 19.00 μN/mm to 32.87 kN/m^2 and 37.38 μN/mm) substrates. Paxillin displacement during contraction on day three was significantly greater in NRVMs attached to soft posts (1.39 μm) compared to flat (1.16 μm) substrates. The volume and time creating 4 dimensional data, interpreted by structural engineering theory, demonstrates subdomain structure is maintained by the counterbalance between the external load acting upon and the internal forces generated by the cardiomyocyte. These findings provide further insight into localized regulation of cellular mechanical function.

Keywords

4D Imaging; Anisotropic Elastic Deformation; Kymograph; Shortening; Shortening Velocity; Traction Force; Surface Stress; Surface Tension

Address reprint requests and inquiries to: russell@uic.edu.

Author Manuscript Author Manuscript Author Manuscript Author Manuscript

1. INTRODUCTION

Heart disorders that affect contractility properties of the cardiomyocyte, including ischemia and hypertrophic cardiomyopathy, can lead to extensive health care costs, lost work productivity and even mortality (Go et al. 2014). When a myocardial infarction (MI) occurs, cardiomyocytes are not delivered the necessary oxygen and many die. The healthy cardiomyocytes that survive an MI are then surrounded by an increased collagen extracellular matrix, which subsequently has decreased elasticity (Borbely et al. 2005). This regionalized stiffened tissue matrix impacts the external forces acting upon the remaining healthy cells, and then the cardiomyocyte internally responds to these localized external mechanical cues.

Variation in cell and tissue stiffness occurs during the contraction/relaxation cycle in healthy and diseased hearts. The maximum heart cell and tissue stiffness is at the end of the systolic shortening during a contraction when blood is ejected. The heart also becomes stiffer with age and disease, which loads all phases of the expansion-contraction process. The cardiac output of the entire heart is a function of the variation in the matrix stiffness (Berk et al. 2007). The stiffness (modulus of elasticity) of the normal adult human heart tissue typically ranges from 10 to 50 kPa (Berry et al. 2006; Bhana et al. 2010; Borbely et al. 2005; Omens 1998) and diseased tissue stiffness from 50 to 500 kPa (Fomovsky et al. 2010; Fomovsky et al. 2010; Holmes et al. 2005). Tissue properties have been mimicked by varying the substrate stiffness, and found to affect cardiomyocyte phenotype (Bhana et al. 2010; Discher et al. 2005; Engler et al. 2008). Substrate stiffness additionally influences the contraction performance of a cardiomyocyte (Engler et al. 2008; Jacot et al. 2008). The external microenvironment stiffness then affects NRVM signaling and the response by contractile sarcomeres occurs in a continuous feedback loop (Berk et al. 2007).

At the sarcomeric level, the cardiomyocyte is composed of protein complexes, such as the sarcomere, composed of thin and thick filaments, titin and the Z-disc, that determine contractile performance of the individual cardiomyocyte. In the aggregate, these contribute to the whole heart function (Solaro et al. 2008). Cardiomyocyte performance is based on the total tension generated internally based on a number of factors, including the external load forces acting upon it. The diseased heart has contractile dysfunction that affects the force-velocity relationship and blood pressure changes (Solaro 2008).

Although some research has been presented on the use of tuning elastomeric material to mimic extracellular matrix and tissue stiffness related to cardiomyocyte function, the impact on performance is not well understood. Cardiomyocytes have been shown to generate more force on stiffer, compared to softer, two dimensional (2D) substrates (Hazeltine et al. 2012; Hersh et al. 2013; Rodriquez et al. 2011; Wang et al. 2011) but few studies have addressed cellular morphology or function when cardiomyocytes are configured in three dimensions (3D) of scaffolds of varying stiffness. Additionally, a clear understanding of the relationship between the external and internal force balancing within subdomains of the NRVM has not been well explained using experimental techniques.

Author Manuscript Author Manuscript Author Manuscript Author Manuscript

We present here the use of microtopography manufactured from a stiffness-tunable elastomeric material providing the cardiomyocyte with a 3D microenvironment. Both live and fixed NRVM studies were conducted to demonstrate how 3D remodeling affects the functional performance over time, known as a four dimensional (4D) system. In these experiments, the micromechanics of NRVM subdomains were assessed by line scan and traction force microscopy to understand the contractility properties and the internal balance of force generated within the cardiomyocyte in response to complex external cues of stiffness and microtopography. These experiments lead to a better understanding of the structure-function relationship in muscle.

2. MATERIALS AND METHODS

2.1 BioMEMS Substrate Fabrication

Fabrication of microtopography substrate surfaces has previously been described by our lab (Motlagh et al. 2003). First, a UV photolithography process using SU-8 photoresist (MicroChem, Newton, MA) on silicon wafers was conducted. The wafers with the manufactured topography surface becomes an initial template thereafter for a parylene template made using a chemical vapor deposition process. The parylene was removed from the wafer and serves as a secondary template to mold topography substrate surfaces on polydimethylsiloxane (PDMS) (Dow Corning, Midland, MI). PDMS was rapidly mixed in a 10:1 or 50:1 elastomer base to curing agent ratio for approximately five minutes. Air bubbles in the bulk PDMS were degassed using a vacuum desiccator for approximately thirty minutes. The bulk PDMS was spun onto cell culture-compatible plates (MatTek, Ashland, MA), which creates a PDMS thickness of approximately 50 microns. For the microtopography substrates, the parylene is placed on PDMS and degassed again for approximately ten minutes. The PDMS substrates were then cured for 24 hours in a 60°C oven. After curing the PDMS, it was cooled and the parylene template was removed leaving PDMS substrates with either a flat or microtopography surface (FIG. 1 a, c).

2.2 Substrate Material Stiffness Testing

Testing of the PDMS substrate stiffness (Young's modulus of elasticity) was conducted using Atomic Force Microscopy (AFM) techniques. Briefly, a new Borosilicate Glass Particle (10 μm) on Silicon Nitride (0.12 N/m) cantilever tip (Novascan, Ames, IA) was used for each experiment session. The tip was first calibrated with respect to a glass surface. Then, six AFM measurements were taken in a region of cured PDMS material along the flat surface of the substrates before relocating the cantilever to a different region for six more measurements, which was repeated three or more times per substrate. Testing of each PDMS elastomer to curing agent mixture to determine the stress-strain properties of the material as related by Young's Modulus of elasticity occurred on a minimum of three samples, from three different mixing batches per PDMS mixture using AFM with a total count of 53 sample points measured for the 50:1 elastomer to curing agent ratio mixture and 41 sample points measured for the 10:1ratio mixture. To analyze micropost related data, the stiffness of the microposts is assumed to be equivalent to the bulk material.

Author Manuscript Author Manuscript Author Manuscript Author Manuscript

2.3 Substrate Preparation for Cell Plating

Substrates were first treated with 5% APTES (3-aminopropyltrimethoxysilane) in a 5% water, 200 proof isopropyl alcohol mixture for 10 minutes. The APTES mixture was aspirated and flushed with 200 proof isopropyl alcohol. The substrates were heated for 25 minutes in a 60° C oven then cooled for 5 minutes before flushing the substrates with a 5% water, 200 proof isopropyl alcohol mixture. When preparing substrates for traction force experiments, an additional step of adding fluorescent microspheres (Life Technologies, Carlsbad, CA) with a 0.5 μm diameter to the surface, as previously described, was applicable (Lateef et al. 2005). Briefly, the beads were combined with a 3.3 mM potassium hydroxide/sterilized water mixture and applied to the substrates for 10 minutes followed by aspiration of remaining liquid to create an approximate 150 bead per 100 square micron adherence (FIG. 1 b, d). The substrates were then coated with a fibronectin (20 μg/ml) in Dulbecco's modified Eagle's medium (DMEM) solution and left in a 37° C, 5% CO_2 incubator for 2 hours prior to seeding cells.

2.4 Cardiomyocyte Culture

Primary cardiomyocyte cultures were obtained from neonatal rat ventricular myocytes (NRVM) according to Institutional Animal Care and Use and NIH guidelines for the care and use of laboratory animals. Hearts were removed and cells were isolated from 1–2 days old neonatal Sprague-Dawley rats with collagenase (Worthington) as previously described (Boateng et al. 2003; Curtis et al. 2013). The cells were re-suspended, filtered through a metal sieve to remove large material and plated at low density (250,000 cells/dish) in a chemically defined, serum-free medium for primary cells (PC-1) (Biowhittaker /Cambrex) on the fibronectin coated substrate surfaces. Cells were left undisturbed for 24 hours in a 37° C, 5% CO_2 incubator. Unattached cells were removed by aspiration and PC-1 media was replenished daily.

2.5 Real-time Phase Imaging

NRVM were imaged under phase microscopy using a Zeiss Laser TIRF 3 Microscope (Zeiss, Peabody, MA) under a 40x objective lens and a 37° C, 5% CO_2 incubator attachment. Cardiomyocytes were filmed with phase microscopy and recorded one frame every five minutes for 24 hours between 18 to 42 hours after plating to view initial attachment and early stage cardiomyocyte remodeling to the micropost. The film was then converted from a 24 hour movie to a playback movie shown over 22 seconds (Online Resource 1).

2.6 Immunohistochemistry

NRVMs were fixed in 10.0 % paraformaldehyde for 10 minutes, followed by a 0.3 M glycine/phosphate-buffered saline (PBS) (Media Tech, Manassas, VA) rinse. NRVMs were then incubated in 0.5 % Triton X-100 (Sigma St. Louis, MO) for 10 min to permeabilize NRVM membranes. NRVMs were labeled with a primary antibody for sarcomeric α-actinin (mouse monoclonal ab9465, Abcam, Cambridge, MA) diluted 1/200 and paxillin (rabbit monoclonal ab32084, Abcam, Cambridge, MA) diluted 1/250 in 1 % Tris-buffered saline – Tween 20 (TBST) (Sigma St. Louis, MO), /1 % Bovine serum albumin (BSA) (Sigma St.

Author Manuscript Author Manuscript Author Manuscript Author Manuscript

Louis, MO) /PBS and left overnight in a 4° F refrigerator. NRVMs were then flushed multiple times with PBS and incubated with mouse anti-rabbit Alexa Fluor IgG 488 and goat anti-mouse Alexa Fluor IgG 568 secondary antibody (Invitrogen) diluted 1/1,000 for 45 min in room temperature. All samples were flushed with PBS then preserved in 1 nM 4',6-diamidino-2-phenylindole (DAPI)/PBS (Vector Labs, Burlingame, CA) and stored in a 4°F refrigerator until imaged.

2.7 Fluorescence Microscopy

NRVM images were captured as 1024 × 1024 pixel images using a Zeiss LSM Observer Z1 microscope (Zeiss, Peabody, MA) with a 63× objective lens for assessment of NRVM surface area using ImageJ (NIH, Bethesda, MA). Z-stacks were gathered with 0.5 μm optical slices and 1024 × 1024 pixel resolution using a Zeiss 710 Confocal Microscope (Zeiss, Peabody, MA) with a 40× or 63× objective lens with laser wavelengths of either 358, 488 or 568 nm, dependent upon the need. Renditions of the Z-stacks to determine variation in NRVM structure with respect to the flat or topography surface were created using Volocity 3D Image Analysis Software (Perkin Elmer, Waltham, MA).

2.8 Fluorescence Voxel Quantification

To quantify focal adhesion localization around microposts, renditions of the Z-stacks were analyzed using Volocity 3D Imaging Analysis Software (Perkin Elmer, Waltham, MA). Briefly, the paxillin fluorescence in cubic micron voxels located around the post (approximately within 2 microns of the post) were regions of interest selected for measurements. The localized paxillin fluorescence voxels were then normalized to the total fluorescence voxels within the cell. Between six and seven cells were measured from three independent experiments per condition.

2.9 Kymograph Analysis for Shortening and Shortening Velocity

The use of a line scan to gain detailed information about myofibrillar contractility was reported by our lab (Curtis et al. 2013). Similar to whole field capture of live NRVMs, spontaneously beating cardiomyocytes were centered in focus under a Zeiss 710 Confocal Microscope (Zeiss, Peabody, MA) with a 25× objective (Zeiss) (FIG. 2 a). Cells were selected based on the following criteria: clusters of two or more were rejected; single cells have a major axis that is visually greater than the minor axis; on micropost substrata cells must be attached at the anchorage site of a major axis. With use of ZEN software (Zeiss) a line scan was taken along the major axis of the cell in the mid height of the myofibril layer. Transmitted light from a differential interference contrast channel was captured from each line every 7.56 ms over the course of 5000 ms, thereby recording multiple complete and regular cycles of NRVM contraction.

From the NRVM-generated motion, peaks of contraction could be easily rendered and used to mark states of maximum shortening and relate such distance to time, as an indicator of shortening velocity, as described by our lab previously (Curtis et al. 2013). Image processing software (LSM Browser, Zeiss) was used to scale the pixel to micron distance as well as the time to obtain the shortening and the associated velocity in single NRVM contractions (FIG 2 b). To calculate maximum shortening, the distance from the start of the

Author Manuscript Author Manuscript Author Manuscript Author Manuscript

contraction to the peak (maximum) shortening was measured and converted from pixel to micron distance. To calculate shortening velocity, the maximum shortening was divided by the time from the start of the contraction to the peak (maximum) shortening. Measurements of shortening and shortening velocity were taken one day after plating for soft and stiff, flat and topography, PDMS substrates. Measurement of the scanned myofibril length was also measured with ImageJ software to produced a scaled value to normalize the shortening and shortening velocity with respect to the myofibril length. Measurements comparing NRVMs plated on soft substrates molded from flat and topography PDMS were also taken at three days after plating. The maximum shortening and associated velocity for NRVM with a major myofibrillar axis was measured for three contractions per NRVM and a total of at least fifteen NRVMs over the course of at least three independent experiments per condition were measured.

2.10 Mapping Diagram of Subdomain Shortening and Shortening Velocity

To understand the NRVM subdomain shortening and shortening velocity, an analysis was performed on a cell that did not have a visually recognizable major myofibrillar axis. With cellular geometry that indicated no dominant major or minor axis, three line scan measurements were taken on three different myofibrils within the cell. Each kymograph was analyzed at five micron increments to determine subdomain shortening and shortening velocity. Each resulting subdomain measurement was transposed onto a visual map as a five micron squared pixel with an incremental color scale to show the subdomain variation. Each measured point is shown with a black outline surrounding the color depicting the respective shortening and shortening velocity range of the subdomain. The adjacent regions to the subdomain pixels are interpreted as having similar subdomain shortening and shortening velocity as a precursor to a finite element analysis approach to modeling the shortening and shortening velocity.

2.11 Traction Force Microscopy for Surface Stress and Surface Tension

To understand the NRVM force generation, the force per area and force per length at the surface interface between the substrate and single NRVM with a major myofibrillar axis were measured using traction force microscopy techniques. NRVMs were compared on 100 kPa topography or flat PDMS at one and three days after plating and the maximum force per area or length was measured. The force per area (surface stress) and the force per length (surface tension) describe the balance of forces at the interface between the substrate and the cell. It is from understanding both of these features that one can characterize the internal-external relationship of forces. Cardiomyocyte contractions were recorded at the interface between the NRVM and substrate surface where 0.5 μm diameter fluorescent beads were plated prior to fibronectin coating on the substrates.

Filming was recorded for 15 images on single scan mode using a 63× magnification, Zeiss LSM Observer Z1 microscope (Zeiss, Peabody, MA). From this time series, a pair of images representing states of rest (diastole) and peak contraction (systole) was selected for later analysis. Images resulting from the data permitted analysis on the force generation related to surface stress and surface tension created by the spontaneous contraction of the cardiomyocyte. Force was measured for three contractions per NRVM and a total of at least

Author Manuscript Author Manuscript Author Manuscript Author Manuscript

fifteen NRVMs were measured over the course of at least three independent experiments per condition. Analysis of the fluorescent bead displacement to define NRVM boundary conditions was conducted with LIBTRC software (Boston U, Boston, MA).

2.12 Paxillin-GFP Transfection and Displacement Analysis

Cells plated on 100 kPa flat or microtopography were transfected with paxillin-GFP (Melendez et al. 2004), by methods previously described for NRVM (Chu et al. 2011). Briefly, after two days after plating, NRVMs were transfected with paxillin-GFP to result in an MOI = 10. On day three, NRVM contractions were recorded using a Zeiss 710 Confocal Microscope (Zeiss, Peabody, MA) with a 40× objective (Zeiss). Experiments were conducted on single NRVMs transfected with paxillin-GFP, which was clearly visible on the bottom of all cells and near the attachment sites of the micropost (for microtopography substrata). Paxillin displacement was detecable and contraction cycles were filmed in the time series scan mode with a pixel dwell time of 1.27 microseconds per pixel. Cells were additionally imaged for line scan analysis as described above. To analyze paxillin displacement, LIBTRC software (Boston U, Boston, MA) was first used to calculate the displacement distances of the paxillin as related by vector arrow distances. The maximum paxillin displacement vector was then measured with ImageJ software to produce a scaled value based on the actual vector arrow. A total of ten cells with at least three comparative contractions were analyzed from three independent experiments per condition.

2.13 Statistical Analysis

Data was organized using Excel software (Microsoft, Redmond, CA) and statistical analysis was performed using GraphPad Prism (GraphPad Software, La Jolla, CA). Differences in quantifiable variables were determined by using either two-tailed Student’s t-test or n-way ANOVA. PDMS stiffness statistics were based on a minimum of three samples per condition and a total of at least 30 sample points were taken. Cellular statistics were based on a minimum sample size of fifteen NRVMs per condition total from a minimum of three experiments per sample set. All NRVM data was expressed as mean ± standard error of the mean (SEM).

3. RESULTS

3.1 Substrate Stiffness

Using the curing time and temperature described in the methods, results define a 50:1 ratio to yield a Young’s Modulus of 98.4 ± 7.36 kPa, while a 10:1 ratio yields a 397.4 ± 30.79, which are rounded off to 100 and 400 kPa, respectively. The 50:1 ratio was the softest PDMS substrate that will mold microposts and retain the micropost shape after removing the parylene and also mimics the upper boundary of normal heart tissue stiffness (Berry et al. 2006; Bhana et al. 2010; Borbely et al. 2005; Omens 1998). The 10:1 ratio has no issue retaining shape after removing the parylene and mimicked tissue stiffness similar to diseased heart tissue (Fomovsky et al. 2010; Fomovsky et al. 2010; Holmes et al. 2005). Stiffness of the two substrata mixtures are significantly different ($p<0.0001$).

Author Manuscript Author Manuscript Author Manuscript Author Manuscript

3.2 Subcellular Structural Influence from Microposts

Real-time imaging of cardiomyocytes after plating was used to observe the adherence of cells to the microtopography in comparison to the behavior on a flat substrate. This is shown with an example of an NRVM attaching to a 100 kPa PDMS micropost, filmed between 18 and 42 hours after plating (Online Resource 1). A thin layer of myofibrils was seen using Z-stack reconfiguration techniques in fixed, immunostained cardiomyocytes on flat substrates for both 100 kPa and 400 kPa stiffnesses (data not shown). However, a deep myofibril layer was observed in the third dimension when the cardiomyocyte was attached to the micropost in both the 100 kPa and 400 kPa substrates (FIG. 3 a–d).The focal adhesions anchored alongside the micropost were able to support the external-internal static load in 3D (Online Resource 2). Furthermore, the NRVM were anchored and generated enough force to move 100 kPa microposts (FIG. 3 e), but not the 400 kPa microposts (FIG. 3 f), during the contraction cycle.

3.3 Cellular Growth of NRVMs

On day one after plating, myofibril length of NRVMs on 100 kPa microposts (41.13 ± 3.03 μm) and flat (49.07 ± 3.54 μm) substrates were similar to those on 400 kPa microposts (40.64 ± 2.19 μm) and flat (48.73 ± 2.91 μm) substrates, respectively (FIG. 4 a). By day three after plating, growth of NRVMs was shown by the myofibril length on 100 kPa microposts (60.69 ± 5.10 μm) and flat (77.73 ± 4.88 μm) substrates, which were were significantly different from day one ($p=0.0022$ and $p<0.0001$, respectively) (FIG. 4 b). NRVMs grew at a similar rate on both the soft and stiff PDMS for both flat and micropost conditions regardless of substrata (FIG. 4 c). There was a statistically significant ($p<0.0001$) hypertrophic growth found from one and three days after plating for both substrate stiffness and topography surface characteristics.

3.4 Localization of Paxillin around Microposts

Paxillin localization, measured in cubic micron voxels from 3D rendered Z-stacks of NRVMs after three days of growth was found to be greater in NRVMs attached to soft microposts (12.04±1.57 percent) compared to stiff microposts (8.18±1.37 percent) ($p=0.08$) (FIG. 4 d).

3.5 Shortening and Shortening Velocity influenced by Substrate Stiffness

Cardiomyocyte maximum shortening and shortening velocity occurs along the major myofibril axis in an inward direction to a centroid region in the NRVM. Maximum shortening was typically the greatest in the region between the anchorage site and the centroid of the NRVM. Cardiomyocyte maximum shortening was greatest on soft posts (1.08 ± 0.05 μm at 4.75 ± 0.25 μm/s) compared to soft flat (0.84 ± 0.04 μm at 3.41 ± 0.16 μm/s), stiff posts (0.66 ± 0.03 μm at 2.88 ± 0.19 μm/s) or stiff flat (0.48 ± 0.02 μm at 1.44 ± 0.10 μm/s) substrates (FIG. 5 a, b) at one day after plating ($p<0.0001$).

3.6 Shortening, Shortening Velocity influenced by Substrate Topography

The influence of stiffness from the external static load was measured for NRVM for one and three days after plating. Shortening and shortening velocity decreased for NRVM on

Author Manuscript Author Manuscript Author Manuscript Author Manuscript

micropost topography between 1 day (1.08 ± 0.05 μm at 4.75 ± 0.25 μm/s) and 3 days (1.04 ± 0.04 μm at 3.85 ± 0.29 μm/s) after plating ($p<0.0001$) (FIG. 5 c, d). Similarly, NRVMs plated on flat substrates had decreased shortening and shortening velocity from one day (0.84 ± 0.04 μm at 3.41 ± 0.16 μm/s) to three days (0.72 ± 0.03 μm at 2.36 ± 0.17 μm/s) after plating ($p<0.0001$) (FIG. 4 c, d). The decrease in these active tension components relate to the increase of the passive tension along the myofibril down to the actin stress cable.

3.7 Normalizing Shortening, Shortening Velocity

Normalization of the maximum shortening and shortening velocity were calculated with respect to the total length of the myofibril to compensate for possible changes due to cell size (Fig 5e–h). Normalization did not affect conclusions of the absolute measures (FIG 5 a–d). At one day maturation after plating, the percent of maximum shortening (FIG 5 e) remained greatest on soft posts (2.62 ± 0.08 percent) compared to soft flat (1.78 ± 0.08 percent), stiff posts (1.76 ± 0.09 percent) or stiff flat (1.03 ± 0.04 percent) substrates ($p<0.0001$). Similarly, the percent of maximum shortening velocity (FIG 5 f) remained greatest on soft posts (11.47 ± 0.46 percent) compared to soft flat (7.28 ± 0.37 percent), stiff posts (7.52 ± 0.46 percent) or stiff flat (3.18 ± 0.28 percent) substrates ($p<0.0001$).

Similarly, the normalized data for maximum shortening and shortening velocity for NRVMs on 100 kPa micropost remained significantly different from one day to three days after plating ($p<0.0001$) (FIG. 5 g, h). The topography decreased maximum shortening and shortening velocity between 1 day after plating (2.62 ± 0.08 percent and 11.47 ± 0.46 percent) to 3 days after plating (1.79 ± 0.11 percent and 7.05 ± 0.76 percent). Likewise, the normalized data for the maximum shortening and shortening velocity for NRVMs on 100 kPa flat topography decreased between 1day after plating (1.78 ± 0.08 percent and 7.28 ± 0.37 percent) to 3 days after plating (0.98 ± 0.05 percent and 3.26 ± 0.30 percent) ($p<0.001$).

3.8 Cardiomyocyte Micromechanics are Subdomain Regulated

Inheterogeneity was analyzed by scanning different myofibrils (FIG. 6 a) and analyzing the subdomain regions of each myofibril at five micron increments. Analyzing subdomain maximum shortening and shortening velocity along each scanned myofibril demonstrates that mechanical function was not equal in each sarcomere when cultured and measured *in vitro* (FIG. 6 b). The subdomain maximum shortening and shortening velocity was then transposed into a mapping diagram (FIG. 6 c, d). This confirmed anisotropic mechanical function within the cardiomyocyte (Buck et al. 2014; Lewinter et al. 2013; Russell et al. 2010; Williams et al. 2013).

3.9 NRVM Force Generation influenced by Time after Plating

Single cardiomyocytes did not have equal and uniform force generation throughout the NRVM when cultured and measured *in vitro*. This subdomain mechanical function of force generation is shown with compiled LIBTRC data regarding surface stress (FIG. 7 a, b) and surface tension (FIG. 7 d, e) for cardiomyocytes plated on flat and micropost substrates, respectively.

Author Manuscript Author Manuscript Author Manuscript Author Manuscript

In the aggregate, on day one after plating, NRVMs generated more maximum surface stress, force per area, when attached to topography (29.12 ± 4.19 kN/m^2) compared to flat (15.36 ± 3.21 kN/m^2) 100 kPa substrates ($p<0.05$) (FIG. 7 c). With NRVM growth, at day three after plating, NRVMs generated a higher maximum surface stress compared to day one after plating for both micropost (42.87 ± 9.49 kN/m^2) and flat substrates (32.87 ± 9.49 kN/m^2) ($p<0.05$) (FIG. 7 c) (n=15 cells with 3 measurements per cell for all experiments). The minimum surface stress found at day one after plating on flat (154.71 ± 39.41 N/m^2) was less than on micropost (170.66 ± 33.03 N/m^2). The minimum surface stress, expectedly, increased by day three for NRVMs on both flat (161.76 ± 37.80 N/m^2) and micropost (217.52 ± 45.01 N/m^2) substrates. The change in minimum surface stress corresponds directly with the change in maximum surface stress found in all conditions on both days for NRVMs (data not shown).

The surface tension, force per length, was greater on micropost (30.11 ± 5.59 μN/mm) compared to flat (19.00 ± 4.92 μN/mm) substrates at day one after plating and increased by day three for both the NRVMs plated on micropost (51.68 ± 14.34 μN/mm) and flat (37.38 ± 9.06 μN/mm) substrates at three days after plating ($p<0.05$) (FIG. 7 f) (n=15 cells with 3 measurements per cell for all experiments). Interestingly, the surface tension output also revealed force generation in the opposite direction of the tension; in other words, compressive force was found in all substrate conditions at an average 1.85 μN/mm (data not shown, p not significant). This compressive force, in the middle region of the NRVM where the contraction equalized, was present in all conditions but not significantly different in any conditions.

3.10 Anchorage Sites in relationship to Myofibril Contractility

A combination of immunohistochemistry, line scan and traction force microscopy experiments, verified the focal adhesions are the structural anchors for the myofibrils. Paxillin, a mechanotransduction protein found within the focal adhesion complex, was used to verify that the anchorage sites were positioned along the micropost (Online Resource 2). The focal adhesion sites that connect the myofibrils aligned parallel to the major-axis of the NRVM generated the greatest force. It is in these major-axis myofibrils that, additionally, the greatest shortening occurs. The overall stability, the combination of active and passive tension within the NRVM, is therefore anchored at the focal adhesion sites. Although these contractility principles occurred in all the cardiomyocytes, most NRVMs demonstrated localized variability between the maximum and minimum force generation within the NRVM, suggesting that cellular mechanics and the balance of forces are locally regulated.

3.11 Focal Adhesion Displacement Related to Subdomain Micromechanics

Paxillin-GFP was transfected into NRVMs on both the flat and micropost substrates of 100 kPa (FIG. 8 a, c). The paxillin displaced within beating NRVMs plated on both the soft flat (Online Resource 3) and soft micropost (Online Resource 4) substrates as shown with playback at 4X the speed of recording. The vector displacement of paxillin-GFP was found using LIBTRC software (FIG. 8 b, d). Simultaneously, multiple line scans were taken on the NRVMs to demonstrate the relationship between shortening, shortening velocity and focal adhesion displacement during the contraction cycle (FIG. 8 e–h) and regionally mapped

Author Manuscript Author Manuscript Author Manuscript Author Manuscript

using the same scale bar (FIG. 8 i) and method as described above. The paxillin-GFP was also analyzed for surface stress (FIG. 8 j, k). The maximum paxillin displacement was greater on the 100 kPa post (1.39 ± 0.06 μm) compared to flat (1.16 ± 0.06 μm) (FIG. 8 l) (p=0.008).

4. DISCUSSION

A major finding of this study was that cardiomyocytes attached in 3D through microtopography have the best contractility properties in terms of shortening and shortening velocity relative to cells plated on flat substrata. An important additional finding is that micromechanical sarcomeric function is subdomain regulated. As cardiomyocytes mature with time after plating on both flat and topography substrates, a decrease of shortening velocity and an increase of both surface stress and surface tension occurs, reflecting an increase of the passive tension along the myofibril. The distribution of paxillin, a component of the focal adheion anchorage, varied slightly around the microposts of two substrate stiffnesses (100kPa and 400kPa). Furthermore, paxillin displacement, observed by a GFP tag, was significantly different with topography structure, demonstating that the focal adhesion sites work in conjunction with the sarcomeric function both in terms of anchorage sites and with active tension. This overall relationship of external cues to trigger internal responses and cellular functional performance can be explained using mechanical principles of structural engineering.

The external environment affects the internal structure and function of the cell, as demonstrated by use of different substrate stiffness in terms of cell spreading, migration, focal adhesion attachment and functional performance (Aratyn-Scaus et al. 2010; Hazeltine et al. 2012; Hersh et al. 2013; Pelham et al. 1997; Oakes et al. 2012; Rodriquez et al. 2011; Samarel 2005; Wang et al. 2011). In the cardiomyocyte, a decrease of shortening and shortening velocity was found through applying different external loads, via the substrate stiffness and the topographic features. Geometric features are critical for maturation of myocyte structure and function (Curtis et al. 2013; Motlagh et al. 2003). For cardiomyocytes, the active tension generated by the actin and myosin interaction is a dynamic system that continually changes during each individual contraction. This impacts the shortening along the myofibril, which has variation down to the individual sarcomeres within the myofibrils (Chapin et al. 2013; Curtis et al. 2013). These variations in the shortening and shortening velocity were also found to affect the associated force generation, leading to the conclusion that contractile function is subdomain regulated.

In the generation of force, an internal balance is necessary and is also found to be subdomain regulated. Mathematically, this localized, subdomain regulation of a cardiomyocyte is best described using both global and local coordinates of an anisotropic elastic body, as modeled with a cell attached to a micropost (Figure 7 a –c). A complete understanding of the contractility elements is divided into both normal and shear subdomains by characterizing the global and local coordinates of the cardiomyocyte. The subdomain shortening, shortening velocity, surface stress and the surface tension can be analyzed with a local coordinate system. Thus, enabling the external-internal balance of forces to be explained during a contraction cycle. The internal force response from the external cues at one point in

Author Manuscript Author Manuscript Author Manuscript Author Manuscript

the cell is balanced in a secondary location, in an equal amount at a symmetric distance away from the equilibrium point within the cell, as described using Maxwell's Reciprocal Theorem (Heyman 2008). The maximum force generation at the focal adhesion on the micropost wall is, therefore, equal to force generation measured along the X-Y plane using force traction microscopy techniques.

The focal adhesions, shown with the paxillin-GFP experiments, demonstrate harmonic dynamic movement in conjunction with sarcomeric shortening and shortening velocity. Likewise, the force per area generated by the focal adhesions displays a similar pattern to displacement. In the aggregate, the contractile dynamics (shortening, shortening velocity, surface stress and surface tension) of NRVMs is greater on soft compared to stiff substrates and simultaneously greater on microposts compared to flat substrates. These contractile dynamics can be modeled with both global and local coordinate system (FIG. 9 a–c). The paxillin, as representative of focal adhesion sites, demonstrates a more dynamic movement and also an increase of anchorage in NRVMs with greater contractile dynamics. The subtle changes of paxillin distribution in the cell and the subsequent displacement of the focal adhesions during contraction show a correlation between anchorage formation and the relationship with respect to myofibril subdomain structure and function. Thus, the counterbalance of forces between the external load acting through the focal adhesions and the internal force generated by myofibrils in the cardiomyocyte permits feedback and interplay of structures and their function resulting in subdomain reorganization within the cell (FIG. 9 d, e).

Physiologically, the balance of forces acting upon and within the cardiomyocyte is critical for effective function. When the mechanics within subcellular zones of muscle cell are asynchronous, the shear stress increases and disrupts the overall myofibril architecture (Yu et al. 2005). In response, the muscle and/or the surrounding connective tissues may attempt to balance the internal force by myofibril assembly and/or by increasing the matrix stiffness externally. Local imbalance, however, may lead to a downstream effect of calcium sparking and eventually to cardiac arrhythmia or heart failure (Cheng et al. 2008). Structural mechanics may further the advancement for understanding the relationship between cellular form and function.

5. SUMMARY

Mechanical attributes of the cardiomyocyte are critical to understand the functional mechanisms in which the cell behaves and responds to its surrounding microenvironment. With changing substrate stiffness, results show that cardiomyocytes contract better on substrates that mimic normal physiologic conditions. The novel use of a combination of stiffness and topography creates a three-dimensional microdomain that mimics a more life-like environment for the cell. NRVMs connected to a micropost grow with myofibrils arranged in with X-Y-Z planes and have increased maximum shortening and shortening velocity.

To analyze cellular mechanics, the cardiomyocyte is recognized as an elastic body with anisotropic characteristics. This affects the active forces produced within the cell, measured

Author Manuscript Author Manuscript Author Manuscript Author Manuscript

by shortening and shortening velocity, and the balance of external to internal active and passive forces, measured by surface stress and surface tension. Subdomain regulation of cellular function is related to its local microenvironment using a combination of line scan and traction force microscopy methods. This quantitative analysis of subcellular forces in cardiomyocytes may be used for clinical research purposes in the future, for example, on human genetic diseases with cardiomyocytes derived from inducible pluripotent stem cells.

Supplementary Material

Refer to Web version on PubMed Central for supplementary material.

ACKNOWLEDGMENTS

We gratefully acknowledge Drs. Shen Sun and Michael Cho for providing assistance with AFM experiments. Gratitude is also extended to Dr. Mark Sussman for providing paxillin-GFP used in these experiments. We also thank Dr. Matthew W. Curtis for his help to customize the method of adhering beads to the substratum surface for the traction force microscopy experiments. Support to conduct this research was provided by NIH NHLBI T32/HL07692, PO/HL62426.

REFERENCES

Aratyn-Schaus Y, Oakes PW, Stricker J, Winter SP, Gardel ML. Preparation of complaint matrices for quantifying cellular contraction. J Vis Exp. 2010; 46(Pii):2173. [PubMed: 21178972]

Berk BC, Fujiwara K, Lehoux S. ECM remodeling in hypertensive heart disease. J Clin Invest. 2007; 117(3):568–575. [PubMed: 17332884]

Berry MF, Engler AJ, Woo YJ, Pirolli TJ, Bish LT, Jayasankar V, Morine KJ, Gardner TJ, Discher DE, Sweeney HL. Mesenchymal stem cell injection after myocardial infarction improves myocardial compliance. Am J Physiol Heart Circ Physiol. 2006; 290(6):H2196–H2203. [PubMed: 16473959]

Bhana B, Iyer RK, Chen WL, Zhao R, Sider KL, Likhitpanichkul M, Simmons CA, Radisic M. Influence of substrate stiffness on the phenotype of heart cells. Biotechnol Bioeng. 2010; 105(6): 1148–1160. [PubMed: 20014437]

Boateng SY, Hartman TJ, Ahluwalia N, Vidula H, Desai TA, Russell B. Inhibition of fibroblast proliferation in cardiac myocyte cultures by surface microtopography. Am J Physiol Cell Physiol. 2003; 285(1):C171–C182. [PubMed: 12672651]

Borbely A, van der Velden J, Papp Z, Bronzwaer JGF, Edes I, Stienen GJM, Paulus WJ. Cardiomyocyte stiffness in diastolic heart failure. Circulation. 2005; 111:774–781. [PubMed: 15699264]

Buck D, Smith JE 3rd, Chung CS, Ono Y, Sorimachi H, Labeit S, Granzier HL. Removal of immunoglobulin-like domains from titin's spring segment alters titin splicing in mouse skeletal muscle and causes myopathy. J Gen Physiol. 2014; 143(2):215–230. [PubMed: 24470489]

Chapin LM, Edgar LT, Blankman E, Beckerle MC, Shiu YT. Mathematical Modeling of the Dynamic Mechanical Behavior of Neighboring Sarcomeres in Actin Stress. Fibers Cell Mol Bioeng. 2014; 7(1):73–85.

Cheng H, Lederer WJ. Calcium sparks. Physiol Rev. 2008; 88(4):1491–1545. [PubMed: 18923188]

Chu M, Iyengar R, Koshman YE, Kim T, Russell B, Martin JL, Heroux AL, Robia SL, Samarel AM. Serine-910 phosphorylation of focal adhesion kinase is critical for sarcomere reorganization in cardiomyocyte hypertrophy. Cardiovascular Research. 2011; 92:409–419. [PubMed: 21937583]

Curtis MW, Budyn E, Desai TA, Samarel AM, Russell B. Microdomain heterogeneity in 3D affects the mechanics of neonatal cardiac myocyte contraction. Biomech Model Mechanobiol. 2013; 12(1):95–109. [PubMed: 22407215]

Discher DE, Janmey P, Wang YL. Tissue cells feel and respond to the stiffness of their substrate. Science. 2005; 310:1139–1143. [PubMed: 16293750]

Author Manuscript Author Manuscript Author Manuscript Author Manuscript

Engler AJ, Carag-Krieger C, Johnson CP, Raab M, Tang HY, Speicher DW, Sanger JW, Sanger JM, Discher DE. Embryonic cardiomyocytes beat best on a matrix with heartlike elasticity: scar-like rigidity inhibits beating. J Cell Sci. 2008; 121(Pt 22):3794–3802. [PubMed: 18957515]

Fomovsky GM, Holmes JW. Evolution of scar structure, mechanics, and ventricular function after myocardial infarction in the rat. Am J Physiol Heart Circ Physiol. 2010; 298(1):H221–H228. [PubMed: 19897714]

Fomovsky GM, Thomopoulos S, Holmes JW. Contribution of extracellular matrix to the mechanical properties of the heart. J Mol Cell Cardiol. 2010; 48(3):490–496. [PubMed: 19686759]

Granzier HL, Irving TC. Passive tension in cardiac muscle: contribution of collagen, titin, microtubules and intermediate filaments. Biophys J. 1995; 68(1):1027–1044. [PubMed: 7756523]

Go AS, Mozaffarina D, Roger VL, Benjamin EJ, Berry JD, Blaha MJ, Stroke SS. Heart disease and stroke statistics – 2014 update: a report from the American Heart Association. Circulation. 2014; 129(3):e28. [PubMed: 24352519]

Hanft LM, Korte FS, McDonald KS. Cardiac function and modulation of sarcomeric function by length. Cardiovasc Res. 2008; 77(4):627–636. [PubMed: 18079105]

Hazeltine LB, Simmons CS, Salick MR, Lian X, Badur MG, Han W, Delgado SM, Wakatsuki T, Crone WC, Pruitt BL, Palecek SP. Effects of substrate mechanics on contractility of cardiomyocytes generated from human pluripotent stem cells. Int J Cell Biol. 2012; 2012:508294. [PubMed: 22649451]

Hersh N, Wolters B, Dreissen G, Springer R, Kirchgebner N, Merkel R, Hoffman B. The constant beat: cardiomyocytes adapt their forces by equal contraction upon environmental stiffening. Biol Open. 2013; 2(3):351–361. [PubMed: 23519595]

Heyman, J. Basic Structural Theory. Cambridge, England: Cambridge University Press; 2008.

Holmes JW, Borg TK, Covell JW. Structure and mechanics of healing myocardial infarcts. Annu Rev Biomed Eng. 2005; 7:223–253. [PubMed: 16004571]

Jacot JG, McCulloch AD, Omens JH. Substrate stiffness affects the functional maturation of neonatal rat ventricular myocytes. Biophys J. 2008; 95(7):3479–3487. [PubMed: 18586852]

Lateef SS, Boateng S, Ahluwalia N, Hartman TJ, Russell B, Hanley L. Three-dimensional chemical structures by protein functionalized micron-sized beads bound to polylysine-coated silicone surfaces. J Biomed Mater Res A. 2005; 72(4):373–380. [PubMed: 15668956]

Lewinter MM, Granzier HL. Cardiac Titin and Heart Disease. J Cardiovasc Pharmacol. 2014; 63(3): 207–212. [PubMed: 24072177]

Melendez J, Turner C, Avraham H, Steinberg SF, Schaefer E, Sussman MA. Cardiomyocyte apoptosis triggered by RAFTK/pyk2 via Src kinase is antagonized by paxillin. J Biol Chem. 2004; 279(51): 53516–53523. [PubMed: 15322113]

Motlagh D, Senyo SE, Desai TA, Russell B. Microtextured substrata alter gene expression, protein localization and the shape of cardiac myocytes. Biomaterials. 2003; 24(14):2463–2476. [PubMed: 12695073]

Oakes PW, Beckham Y, Stricker J, Gardel ML. Tension is required but not sufficient for focal adhesion maturation without a stress fiber template. J Cell Biol. 2012; 196(3):363–374. [PubMed: 22291038]

Omens JH. Stress and strain as regulators of myocardial growth. Prog Biophys Mol Biol. 1998; 69(2–3):559–572. [PubMed: 9785956]

Pelham RJ, Wang YL. Cell locomotion and focal adhesions are regulated by substrate flexibility. Proc Natl Acad Sci. 1997; 94:13661–13665. [PubMed: 9391082]

Rodriquez AG, Han SJ, Regnier M, Sniadecki NJ. Substrate stiffness increases twitch power of neonatal cardiomyocytes in correlation with changes in myofibril structure and intracellular calcium. Biophys J. 2011; 101(10):2455–2464. [PubMed: 22098744]

Russell B, Curtis MW, Koshman YE, Samarel AM. Mechanical stress-induced sarcomere assembly for cardiac muscle growth in length and width. J Mol Cell Cardiol. 2010; 48(5):817–823. [PubMed: 20188736]

Samarel AM. Costameres, focal adhesions, and cardiomyocyte mechanotransduction. Am J Physiol Heart Circ Physiol. 2005; 289(6):H2291–H2301. [PubMed: 16284104]

Author Manuscript Author Manuscript Author Manuscript Author Manuscript

Solaro RJ, deTombe P. Review focus series: sarcomeric proteins as key elements in integrated control of cardiac function. Cardiovasc Res. 2008; 77(4):616–618. [PubMed: 18192242]

Wang PY, Yu J, Lin JH, Tsai WB. Modulation of alignment, elongation and contraction of cardiomyocyte through a combination of nanotopography and rigidity of substrates. Acta Biomater. 2011; 7(9):3285–3293. [PubMed: 21664306]

Williams CD, Salcedo MK, Irving TC, Regnier M, Daniel TL. The length-tension curve in muscle depends on lattice spacing. Proc Biol Sci. 2013; 280(1776):20130697. [PubMed: 23843386]

Yu J, Russell B. Cardiomyocyte remodeling and sarcomere addition after uniaxial static strain in vitro. J Histochem Cytochem. 2005; 53(7):839–844. [PubMed: 15995142]

Author Manuscript Author Manuscript Author Manuscript Author Manuscript

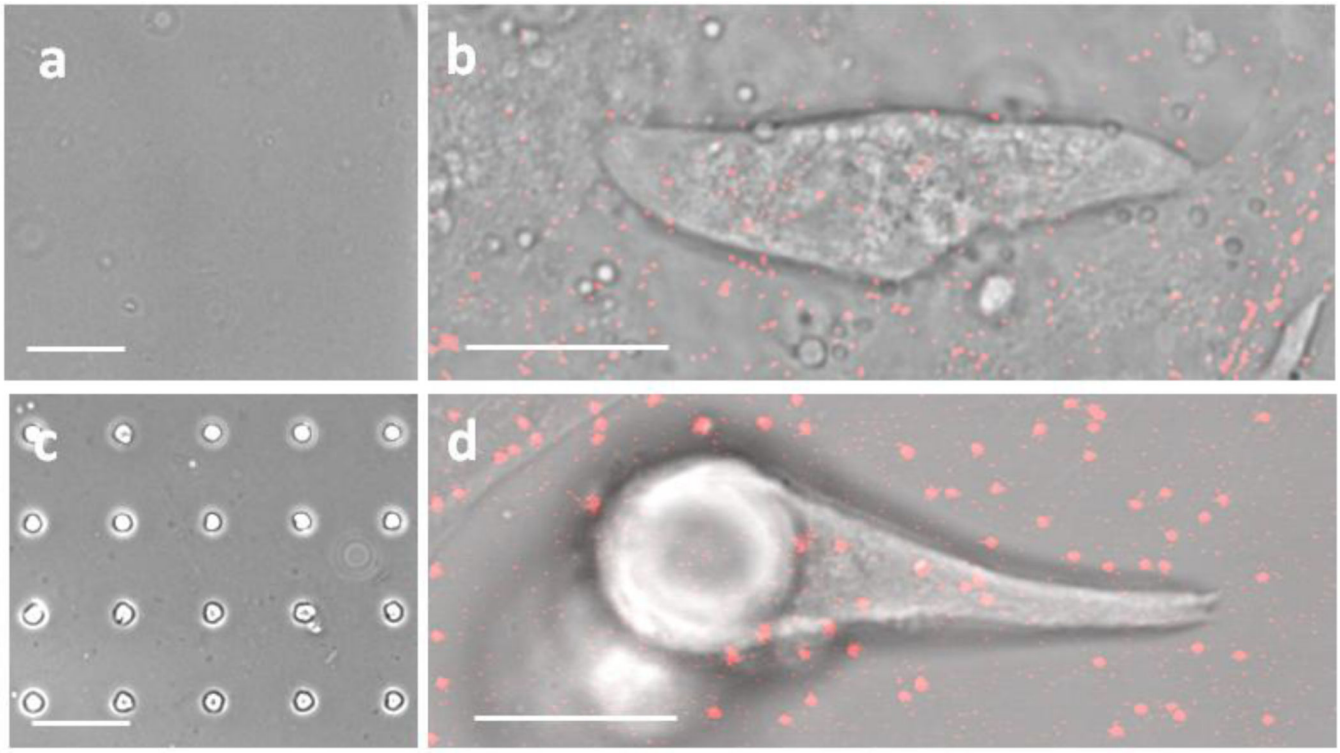

Figure 1. Experimental set-up using PDMS with or without Microposts for Contractility experiments of Neonatal Rat Ventricular Myocytes (NRVM)

(a) Flat PDMS, (b) NRVM seeded on flat PDMS with fluorescent microbeads attached to the substrate, (c) Micropost topography PDMS, (d) NRVM seeded and attached to micropost with fluorescent microbeads attached to the substrate, (a, c) scale = 75 μm. (b, d) scale = 15 μm.

Author Manuscript Author Manuscript Author Manuscript Author Manuscript

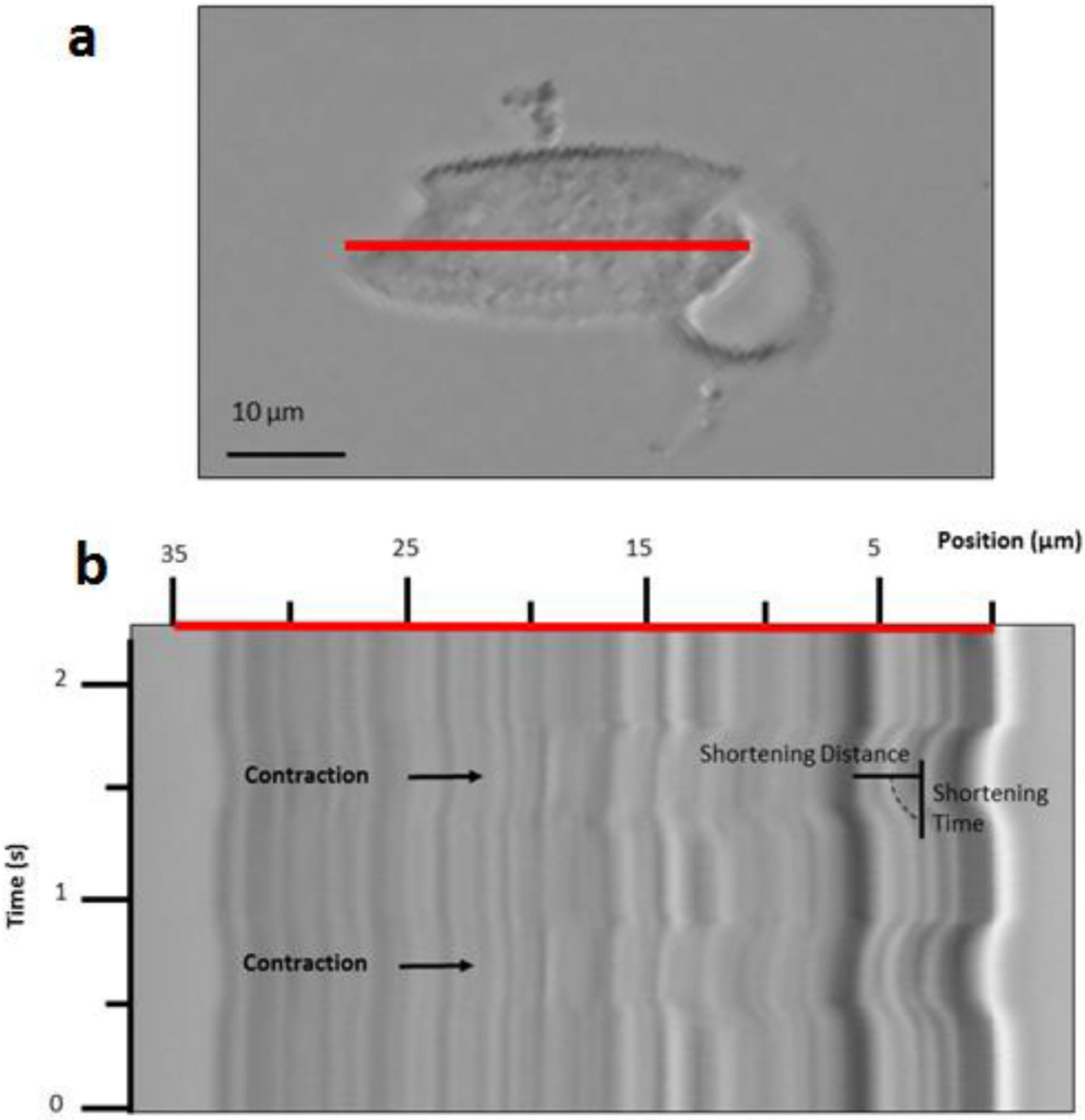

Figure 2. Measuring Shortening and Shortening Velocity using a Kymograph

(a) Motion recorded within a single NRVM on a 100 kPa Post, 1 day after plating, via a line scan (red line). (b) Kymograph of axial cell displacements (red line scanned over time) yields maximum shortening, at which maximum shortening time is measured.

Author Manuscript Author Manuscript Author Manuscript Author Manuscript

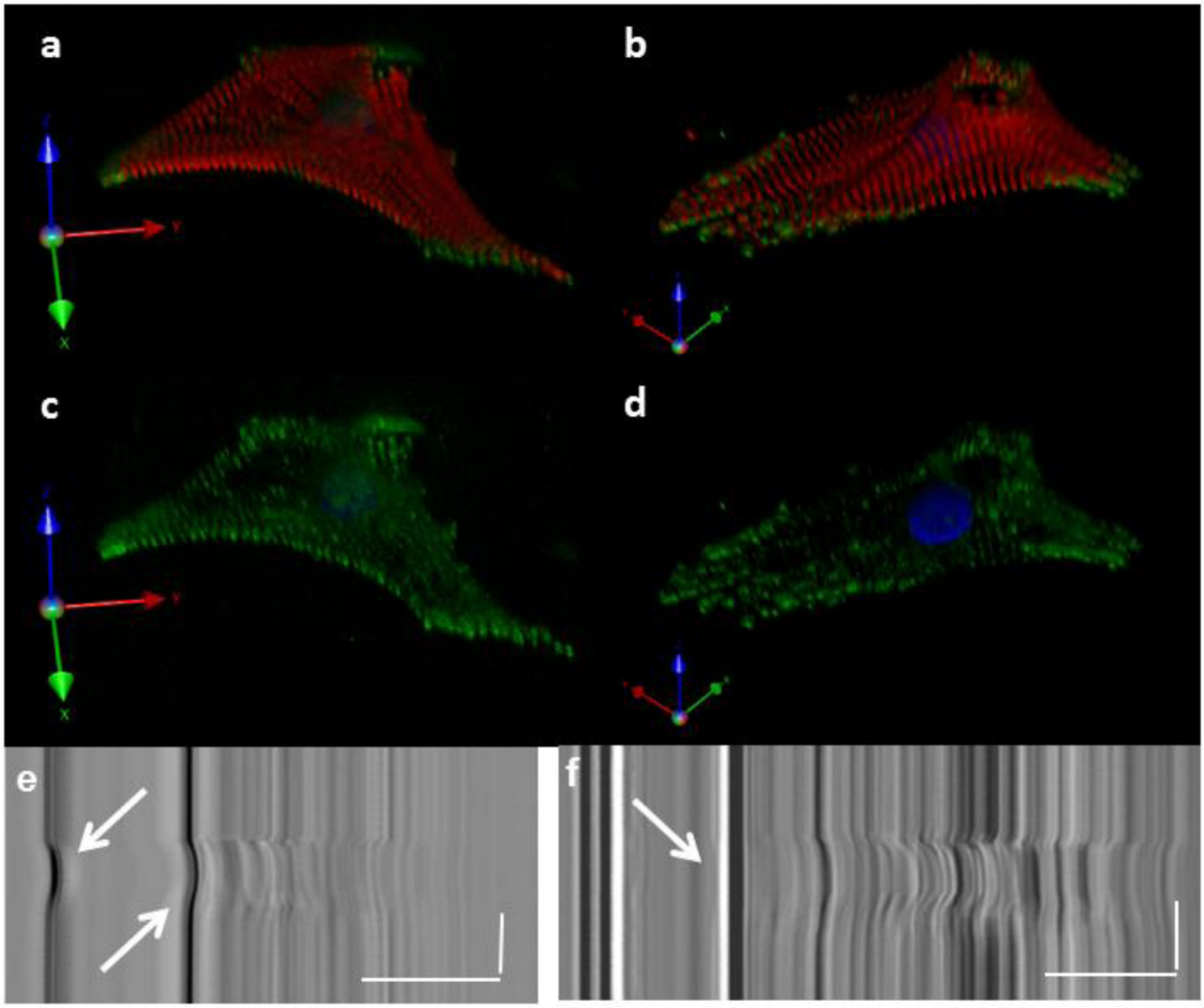

Figure 3. Myofibril Structural Remodeling of NRVM in response to Micropost Topography

Z-stack reconstruction of a cell plated on 100 kPa (a, c) or 400 kPa (b, d) at 3 days after plating. NRVM fixed and stained for myofibril structure (alpha-actinin, red), focal adhesions (paxillin, green) and nucleus (DAPI, blue). Posts are black holes in the upper right region of the cells. (e) NRVM is capable of displacing a 100 kPa micropost, arrows. (f) NRVM does not displace 400 kPa microposts, arrow. (a–d) Distance scale = 20 μm. (e, f) Distance scale = 15 μm, Time Scale = 1 s.

Author Manuscript Author Manuscript Author Manuscript Author Manuscript

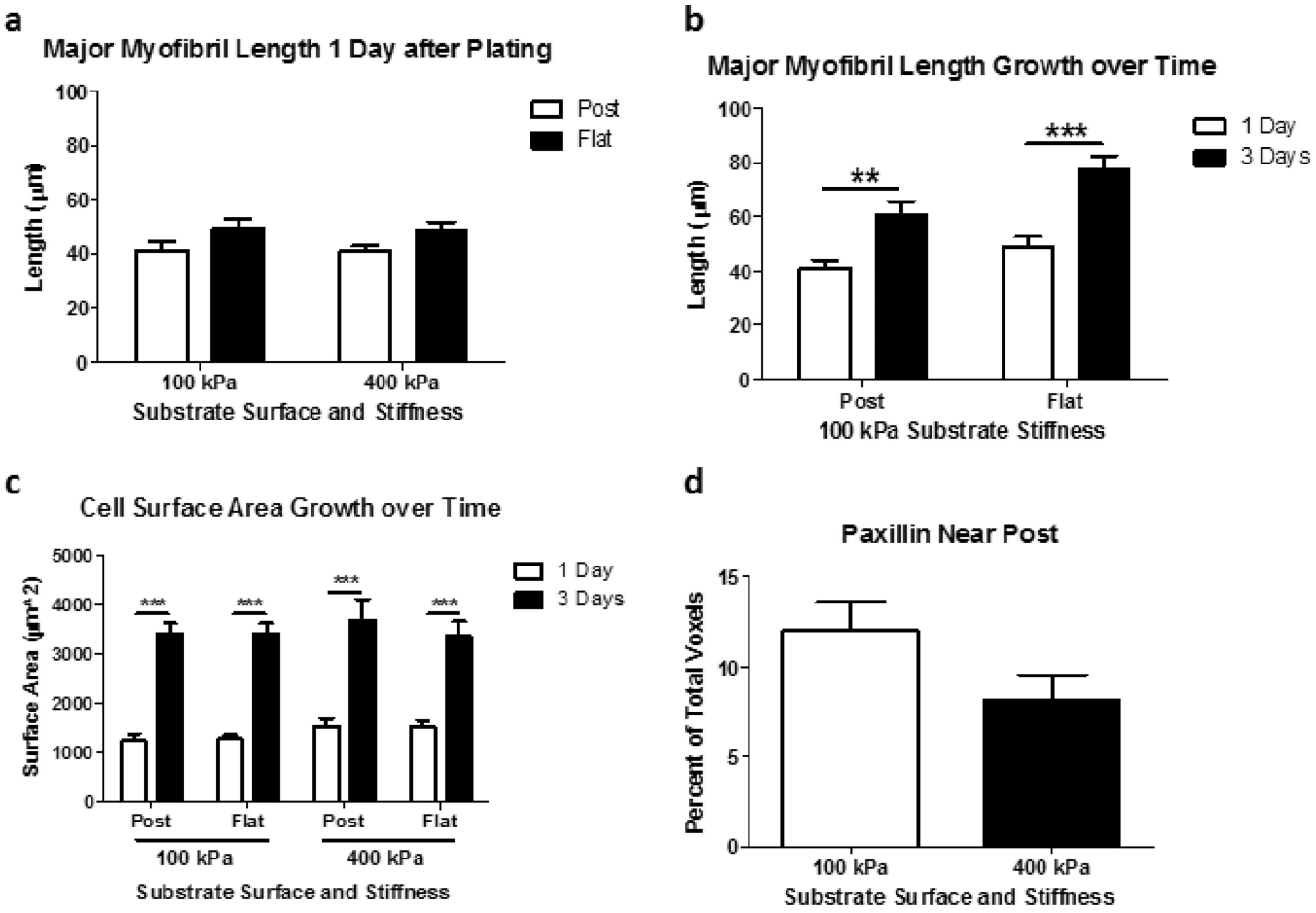

Figure 4. NRVM Grow at a Similar Rate over Time on Micropost and Flat Substrata

(a) Major myofibril length after one day of growth is similar for NRVMs plated on either 100 or 400 kPa of micropost or flat substrata. (b) Major myofibril length after three days of growth is statistically significant over time but not significant for the micropost or flat substrates. (c) NRVM surface area growth was also found to not be statistically different relative to substrate surface plated upon but relative to time. (d) Paxillin localized more around 100 kPa compared to 400 kPa microposts after three days of growth (p=0.08). (a,b) N=15 cells per condition from 3 experiments; (c, d) n=7=8 cells per condition from 3 experiments. Statistical Significance: ** p<0.01; *** p<0.0001.

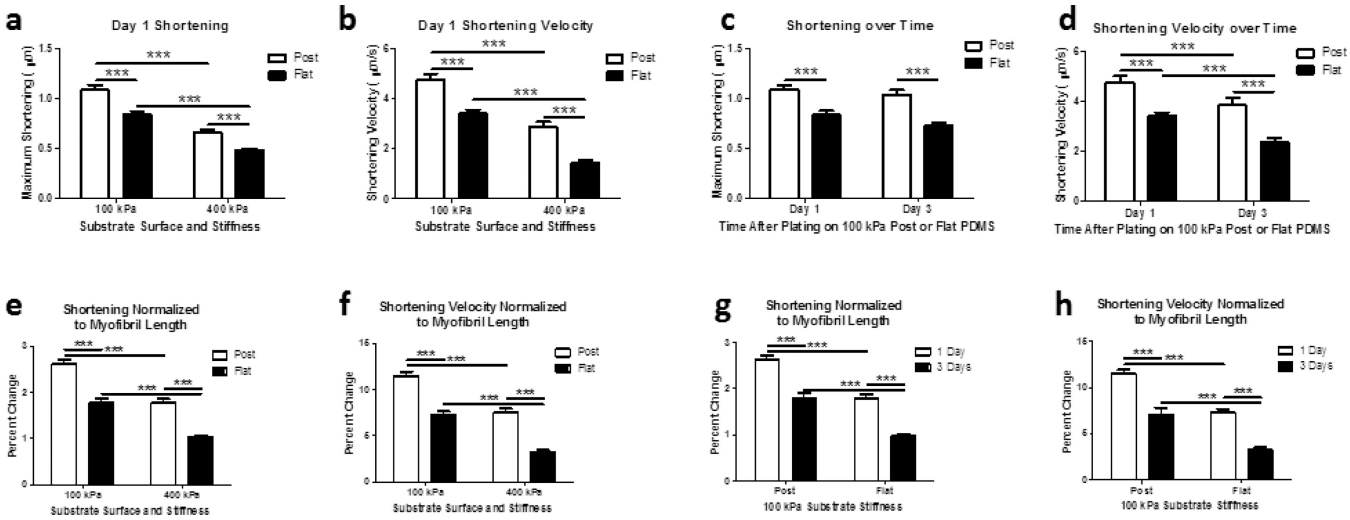

Figure 5. NRVM Shortening and Shortening Velocity is Improved with 3D Micropost Configuration

(a) Maximum shortening one day after plating indicates NRVMs on softer, topography structures shorten the greatest, whereas NRVMs on flat stiff substrates shorten the least. (b) NRVMs shortening velocity performance is similarly related to shortening. (c) Maximum shortening three days after plating indicates NRVMs shorten similarly to that found one day after plating. (d) NRVMs shortening velocity decreases over time between one and three days after plating. (e–h) NRVM shortening and shortening velocity normalized to the length of the myofibril demonstrates functional improvement when cells are configured in three-dimensions with softer microposts.(a–h) N=15 cells per condition with 3 contraction samples per cell for line scans. Statistical Significance: *** $p<0.0001$.

Author Manuscript Author Manuscript Author Manuscript Author Manuscript

Author Manuscript Author Manuscript Author Manuscript Author Manuscript

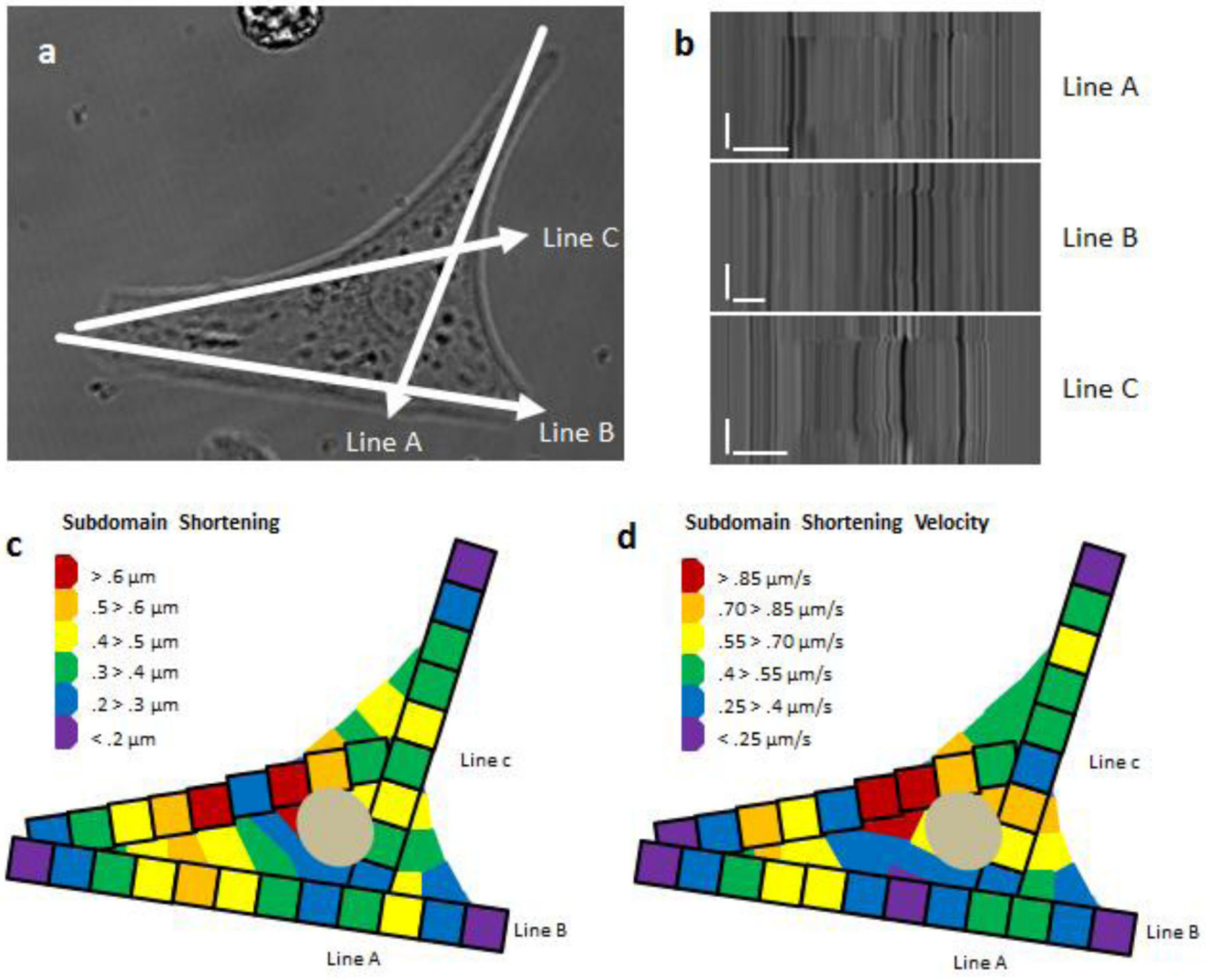

Figure 6. Subdomain Shortening and Shortening Velocity within the Cardiomyocyte

(a) Three different myofibrils were scanned using line scan microscopy within a single cardiomyocyte plated on a 400 kPa flat substrate. (b) Raw data of each myofibril line scan was then analyzed in five micron increments to determine shortening and shortening velocity within the subdomains of the cardiomyocyte. (c, d) Subdomain shortening at each position was then transposed as a 5 × 5 micron square as depicted with a black outline box per each subdomain; the remaining cell region is interpreted to have shortening and shortening velocity similar to the adjacent subdomain. (B) Scale Bars: Distance = 10 microns; Time = 1 second.

Author Manuscript Author Manuscript Author Manuscript Author Manuscript

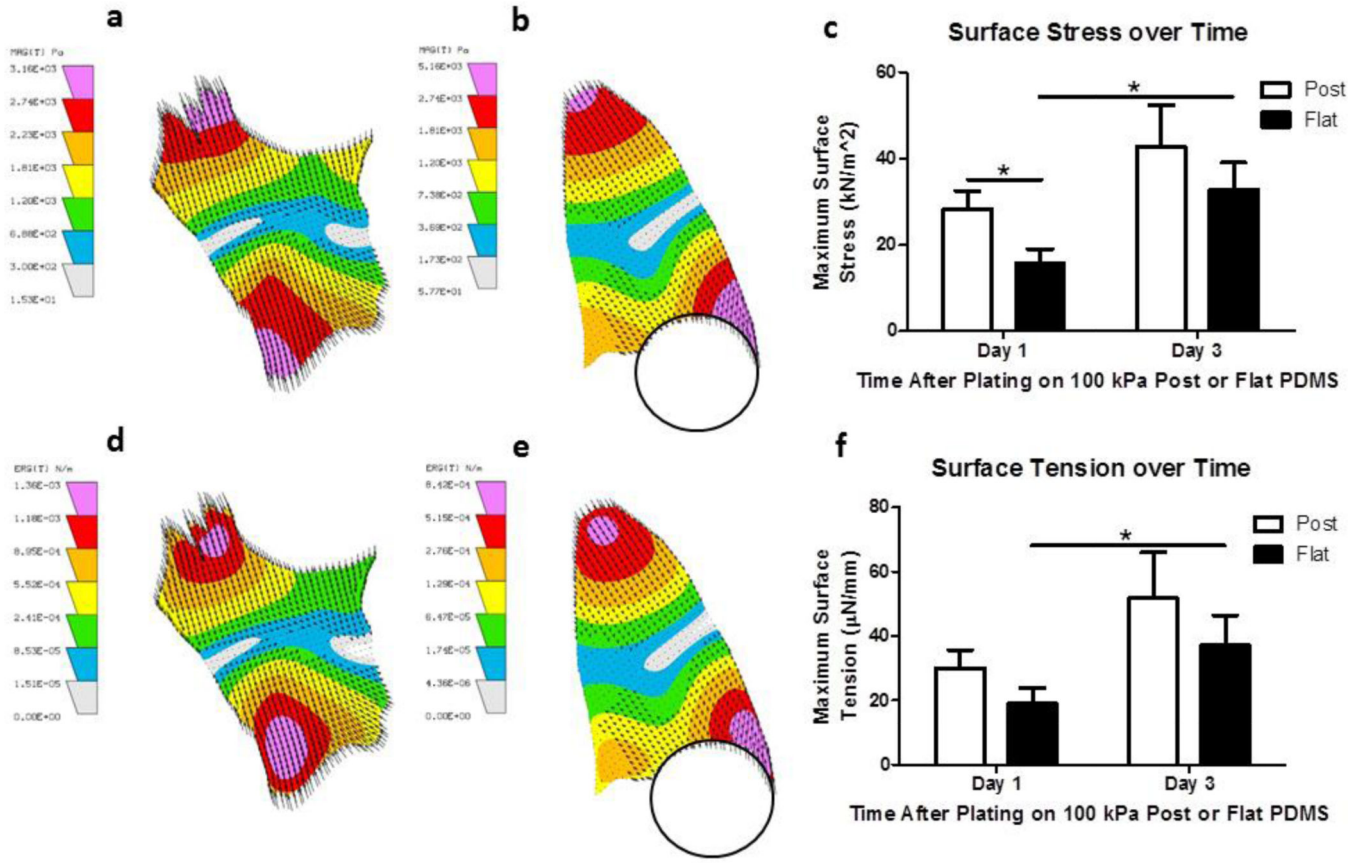

Figure 7. NRVM Force Generation influenced by Maturation Time after Plating

(a, b) Balance of surface stress within NRVM plated on flat and topography substrata, respectively. (c) Compiled maximum surface stress found in NRVM plated on micropost or flat substrata and compared one and three days after plating. (d, e) Balance of surface tension within NRVM plated on flat and topography substrata, respectively. (f) Compiled maximum surface tension found in NRVM plated on micropost or flat substrata and compared one and three days after plating. (c, f) N=15 cells per condition with 3 contraction samples per cell from at least three experiments reported per condition. Statistical Significance: * $p<0.05$.

Author Manuscript Author Manuscript Author Manuscript Author Manuscript

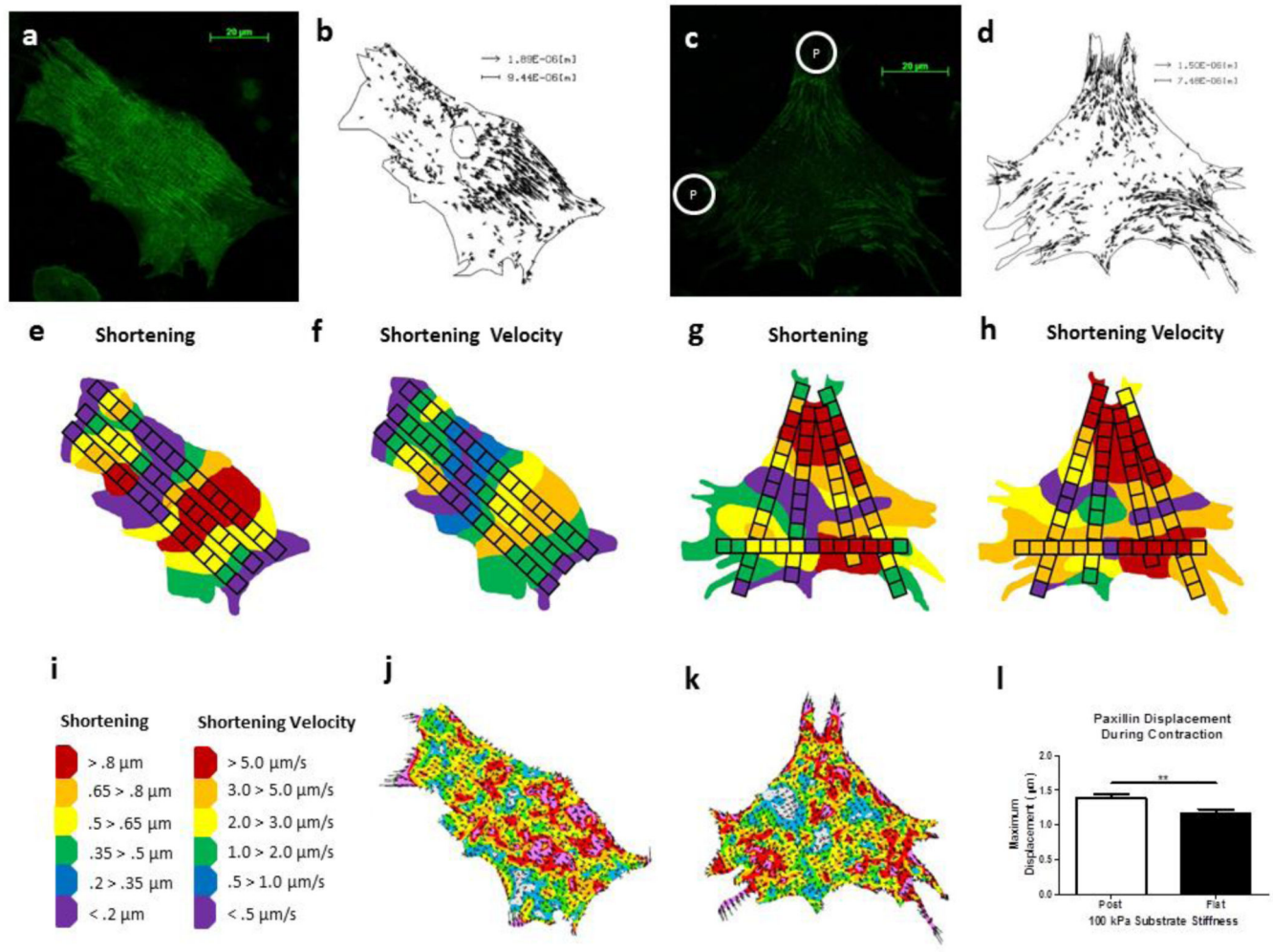

Figure 8. Paxillin Displacement Related to Subdomain Contractility

(a, c) Paxillin-GFP was transfected into NRVMs plated on 100 kPa flat or micropost (P) topography substrata, respectively, and measured after three days of growth. (b, d) Paxillin-GFP displacement was measured using LIBTRC software. (e–h) Line scans were taken to measure shortening and shortening velocity in the same cell. (i) Using an identical scale, shortening velocity was greater in the NRVM plated on micropost topography. (j, k) Force per area within NRVMs was greater in subdomain regions where paxillin-GFP displaced and shortening/shortening velocity was more active, as defined with a surface stress magnitude similar to that observed using microbeads. (l) Maximum paxillin-GFP displacement was greater in NRVMs configured on microposts compared to flat substrates, N=10 cells with 3 contraction samples per cell from at least three experiments reported per condition. Statistical Significance: ** p=0.008.

Author Manuscript Author Manuscript Author Manuscript Author Manuscript

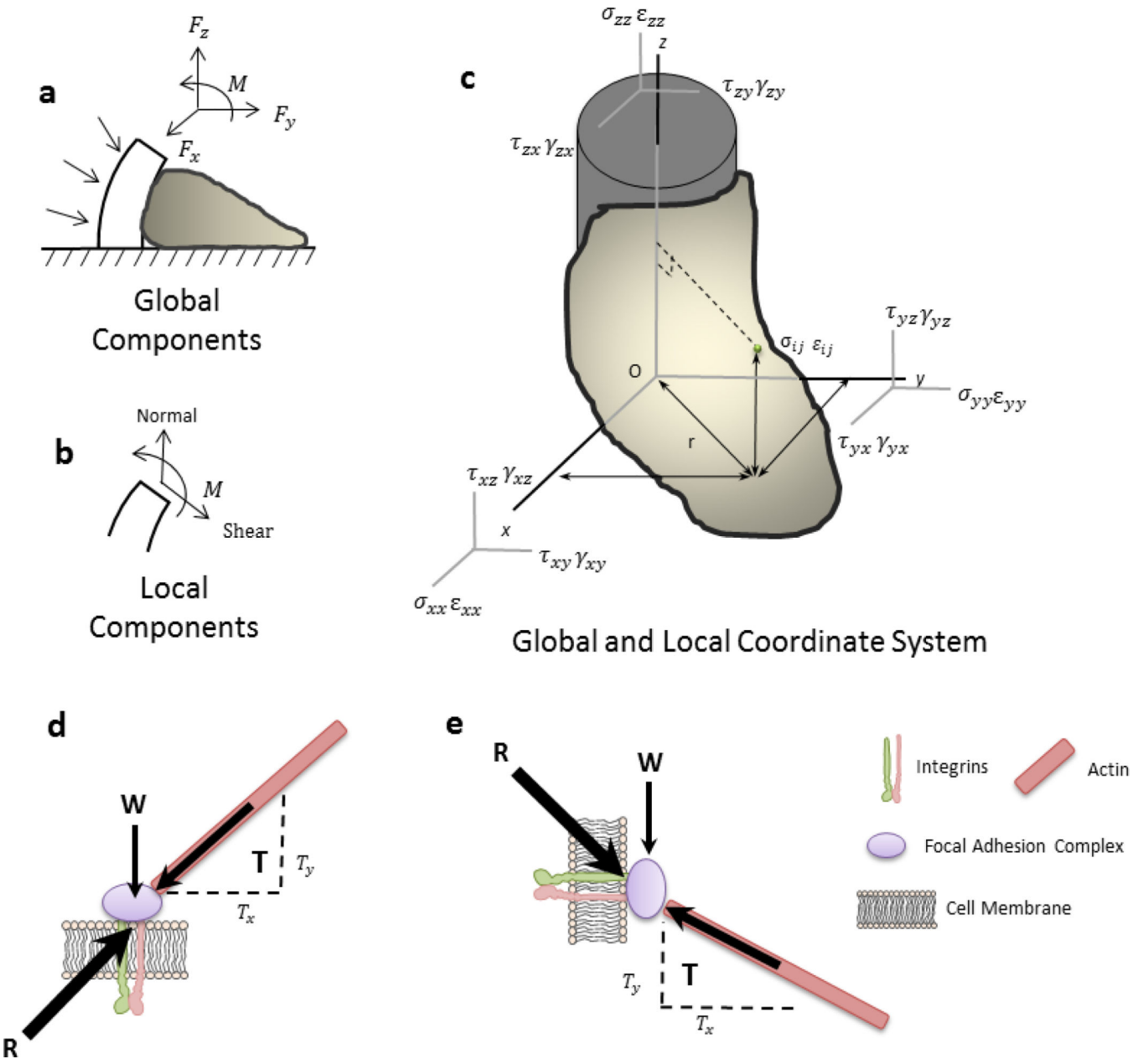

Figure 9. Schematic Representation of the Global and Local Coordinate System within a Cell

(a) Under 3D conditions, the external forces act against the cell but improve the microenvironment for function, such as cardiomyocyte shortening. (b) Global components are divided into local components in their respective x, y and z elements. (c) The global and local coordinate system is used to relate the external environment to the internal forces and displacement to determine the stability of the cell. (d, e) The resultant force acting upon a focal adhesion is localized differently in a cell configured in two- compared to three-dimensions.